BOLETIN DE LA SOCIEDAD ESPAÑOLA DE
Cerámica y Vidrio
www.elsevier.es/bsecv

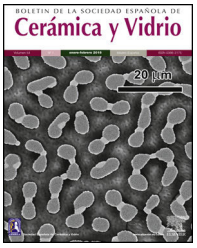

Sustainable glasses in the SiO_2–P_2O_5–CaO–K_2O system from waste and concentrated solar power

Maximina Romero[a,*], *Isabel Padilla*[a], *Luisa Barbieri*[b], *Fernanda Andreola*[b], *Aurora López-Delgado*[a]

[a] *Eduardo Torroja Institute for Construction Sciences, IETcc-CSIC, Madrid, Spain*
[b] *University of Modena and Reggio Emilia, Department of Engineering "Enzo Ferrari", Modena, Italy*

ARTICLE INFO

Article history:
Received 13 October 2021
Accepted 29 December 2021
Available online 7 January 2022

Keywords:
Concentrated solar power
Animal bone flour ash
Packaging glass cullet
Green glass production
Fertilizing glass

ABSTRACT

Sustainable glasses were prepared by green technology including the use of different wastes as raw materials and concentrated solar power (CSP) as renewable energy. The raw materials used to formulate the glasses were animal bone flour ash, which presents high contents of CaO, P_2O_5 and alkaline oxides; glassy sand from the waste of packaging glass submitted to a primary treatment, composed principally of SiO_2; and potassium carbonate of reagent grade. Different exposure times to solar radiation were tested. For comparison, the same composition of glass was melted into a conventional electric furnace. The use of CSP to produce glasses reduces the melting time by approximately 90%, with consequent energy savings. The increased CSP processing time results in more amorphous and thermally stable glasses. The results showed the viability of producing ecofriendly glasses in the SiO_2–P_2O_5–CaO–K_2O system, which could be used as matrix-based fertilizers.

Vidrios sostenibles en el sistema SiO_2-P_2O_5-CaO-K_2O a partir de residuos y radiación solar concentrada

Palabras clave:
Radiación solar concentrada
Cenizas de hueso
Casco de vidrio de envase
Producción sostenible
Vidrio fertilizante

RESUMEN

Se prepararon vidrios sostenibles mediante una tecnología alternativa que incluye el uso de diferentes residuos como materias primas y energía solar concentrada (ESC) como fuente de energía renovable. Las materias primas utilizadas para formular los vidrios fueron ceniza de harina de hueso animal, que presenta altos contenidos de CaO, P_2O_5 y óxidos alcalinos; arena vítrea procedente de residuos de envases de vidrio sometidos a un tratamiento primario, compuesta principalmente por SiO_2, y carbonato potásico de grado reactivo. Se evaluó el efecto del tiempo de exposición a la radiación solar sobre las características de los vidrios obtenidos. Como material de referencia se empleó un vidrio de la misma composición obtenido en un horno eléctrico convencional. El uso de la ESC para producir vidrios reduce

* *Corresponding author.*
E-mail address: mromero@ietcc.csic.es (M. Romero).
https://doi.org/10.1016/j.bsecv.2021.12.004

el tiempo de fusión en aproximadamente un 90%, con el consiguiente ahorro de energía. El aumento del tiempo de procesamiento da lugar a vidrios más amorfos y de mayor estabilidad térmica. Los resultados mostraron la viabilidad de la producción de vidrios sostenibles en el sistema SiO_2-P_2O_5-CaO-K_2O, que podrían utilizarse como fertilizantes.

Introduction

The increase in population and industrial activities, while producing goods, services and materials that favor economic growth and contribute to our modern living standards, can nevertheless negatively impact our environment and well-being. When addressing waste management, a quantitative increase in their generation and important management problems related to their heterogeneity is observed. Regulatory policies have been introduced within the European Union to control and minimize the related impacts and develop a model that can also lead to economic benefits while protecting the environment and human health. The circular economy is the answer to the "take-make-dispose" concept of the linear economy, and it aims to reduce the generation of waste through biological, technical or commercial cycles. Moreover, the use of waste or byproducts as raw materials within open-loop recycling is a good practice recommended by the European Community in the legislative field. In this regard, considerable research has been carried out aimed to the re-use of waste in the manufacture of different materials such as, glass and ceramic materials [1–9], mortars [10,11], geopolymers [12], gypsum [13] or lime [14], among others.

On the other hand, the alarming increase in CO_2 emissions to the atmosphere encourages urgent changes toward less contaminant systems to produce energy. Such a high concentration of global CO_2 of 413 ppm was recorded by the American National Oceanic and Atmospheric Administration for September 2021 [15]. This is a worrying situation, and accordingly, changes in our production systems must be highly considered.

Both the use of waste and the reduction of CO_2 emissions have been taken into account in the Sustainable Development Goals for 2030 [16], which are the blueprint to achieve a better and more sustainable future. Thus, targets of SDGs are substantially increase the reuse of waste (Goal 12 – Responsible consumption and production) and reducing CO_2 levels and other greenhouse gases in the atmosphere (Goal 13 – Climate action).

Sustainable agriculture is also a target of the SDGs, which aim to ensure sustainable food production systems that progressively improve land and soil quality. Given this scenario, research on developing new controlled-release fertilizers (CRFs) has been encouraged worldwide in the last years. The use of CRFs can help to mitigate the problem of soil contamination from the abusive use of traditional mineral fertilizers (ammonium nitrate or urea, ammonium phosphate, potassium chloride, etc.), due to the need to use large quantities to have a good yield harvest [17]. Fertilizing glasses are a type of matrix-based fertilizer, in which nutrients (N, P, K, Ca or Mg) are included in the glassy network and they are gradually solubilized [18]. Some research has reported the manufacture of fertilizing glasses containing the main nutrients P and K prepared from pure reagents [19,20].

In recent decades, the use of renewable energy sources instead of traditional ones for high energy demanding processes has received great attention. In this sense, the use of concentrated solar radiation for high-temperature processes has been most investigated. Among its advantages, it is almost limitless energy and does not produce greenhouse gases, and concentration technologies have quickly developed for high-temperature industrial processes. Research studies conducted to obtain glasses by using concentrated solar power (CSP) have scarcely been performed. In this sense, the authors have recently studied the use of CSP to produce glass frits with excellent results related to the characteristics of the obtained materials in comparison to those obtained by conventional processes [21,22].

In previous papers, the authors demonstrated the possibility of obtaining fertilizing glasses in the SiO_2–P_2O_5–CaO–K_2O system by using alternative raw materials and low-cost products from the perspective of the circular economy [23–25]. Such active glasses were obtained through an energy-intensive conventional melting process, which leads to high CO_2 emissions due to the use of fossil fuels [26].

With the aim of contributing to the conservation of natural resources, the re-use of waste and, also to the decrease of the CO_2 emission derived to the use of non-renewable energy, this research focuses on the production of glasses in the SiO_2–P_2O_5–CaO–K_2O system from waste as raw materials (animal bone flour ash and packaging glassy sand from municipal solid waste) by providing the energy required to melt the glass through concentrated solar radiation. To our knowledge, this is the first time that such a study has been undertaken.

Materials and methods

Raw materials

The raw materials used to prepare glasses in the SiO_2–P_2O_5–CaO–K_2O system were animal bone flour ash, glassy sand and K_2CO_3 (reagent grade). Animal bone flour ash presents high contents of CaO (42.1 wt.%) and P_2O_5 (29.2 wt.%), as well as other oxides such as Na_2O (3.9 wt.%), SiO_2 (1.7 wt.%), K_2O (2.7 wt.%) and MgO (1.4 wt.%). It consists principally of inorganic and nontoxic compounds such as $Ca_5(PO_4)_3OH$ (hydroxyapatite), $CaCO_3$ (calcite) and $Ca_9MgK(PO_4)_7$. Glassy sand is an end of waste coming from the secondary treatment of the waste (19 12 05 EWC code) of the primary treatment of packaging glass. This raw material is produced by an authorized plant in northern Italy and consists of sodium-calcium

Table 1 – Theoretical chemical composition (wt.%) of the studied glass.

SiO_2	Al_2O_3	Na_2O	K_2O	CaO	MgO	P_2O_5	Fe_2O_3	PbO	TOT
31.90	0.90	6.32	14.56	27.29	1.46	17.47	0.01	0.03	99.94

Table 2 – Experimental conditions for the exposure of the sample to concentrated solar radiation.

Shutter opening (%)	Power (W)	FG_{15} t (min)	FG_{20} t (min)	FG_{30} t (min)	FG_{35} t (min)
30	150	2	2	2	2
50	350	3	3	3	3
60	480	5	5	5	5
70	600	3	5	5	5
90	890	–	–	10	10
100	970	2	5	5	10
t_{total} (min)	–	15	20	30	35

silicate glass (SiO_2, 71.3 wt.%; CaO, 10.0 wt.%; Na_2O, 12.7 wt.%; MgO, 2.2 wt.%; Al_2O_3, 2.0 wt.% and other minor oxides). The characterization of raw materials has been previously reported [23].

Glass preparation

A mixture of animal bone flour ash (40 wt.%), glassy sand (42 wt.%) and K_2CO_3 (18 wt.%) were formulated to get a glass with the theoretical composition shown in Table 1. This glass composition was previously tested as fertilizing glass [23]. The mixture of the raw materials was homogenized in a ball mill for 15 min. The melting of the batches was performed using concentrated solar power (CSP) under different process parameters in a Medium Size Solar Furnace (MSSF) located in the CNRS-PROMESS Solar facilities (Font Romeu-Odeillo, France). The solar furnace of 0.9 kW equipped with a vertical axis parabolic reflector of 1.5 m diameter produces a focal spot, approx. 15 mm in diameter, with a very high power density (1000 W m^{-2}). To control the incident solar radiation, a shutter is positioned between the parabolic concentrator (placed on a 6th floor level) and the heliostat (placed on a first floor level). This vertical configuration is the only configuration that allows the heat treatment of powdered materials. A picture showing the configuration of the CSP system has been previously reported [21,22].

During the experiments, solar normal direct irradiation was quasi-steady, and values between 837 and 895 W m^{-2} were registered. Batches were placed in cylindrical (22 mm diameter and 25 mm high) silicon-aluminous crucibles. The temperature was measured by a type K thermocouple, which was positioned into a hole located at half the height of the crucible wall. The shutter was partially opened (30%) at the beginning of the experiments to avoid an abrupt increase in temperature on the sample; immediately after, the shutter was progressively opened until the temperature was approximately 1300 °C, and the mixture was completely melted. Nevertheless, the temperature inside the bulk melt is supposed to be much higher, but its direct measurement was not able due to work limitations. Table 2 collects the experimental conditions related to the shutter opening percentage and the time of exposure to concentrated solar radiation of different samples. Hereafter, the samples melted with CSP are named

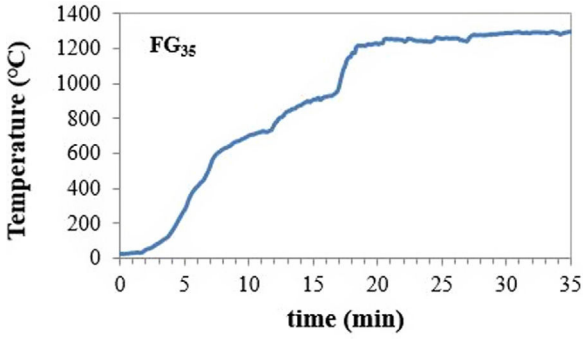

Fig. 1 – Temperature–time schedule used for melting raw materials with CSP.

FG_x, where x is the time of exposure to solar radiation (15, 20, 30, and 35 min).

An example of the temperature-time register followed for the experiment to produce glass frits with CSP is shown in Fig. 1. The inflection points in the curve correspond to the successive opening of the shutter (see Table 2).

To compare the properties of glasses obtained by CSP and traditional melting, a glass referred as FG_T was prepared in a conventional electric furnace. The batch was heated at 20 °C min^{-1} to 900 °C, where an isotherm was maintained for 60 min for raw material degasification. Subsequently, the batch was heated at 10 °C min^{-1} to 1450 °C and held for 120 min.

After thermal schedule, melts obtained in both the electric furnace and by CSP were quenched in cold water and subsequently dried and characterized.

Glass characterization

Glasses were characterized to determine whether the type of energy, power density, and thermal schedule used in their preparation led to materials with similar physical-chemical characteristics. The chemical analysis of samples was determined by X-ray fluorescence (XRF) using a Bruker S8 Tiger spectrometer. The analysis was performed on pressed pellets of powder glass samples (< 63 μm). The evaluation of the amorphous or crystalline nature of samples after melting was

Fig. 2 – Macroscopic appearance of glass frit.

performed by X-ray diffraction (XRD) using Bruker D8 Advance equipment with Ni-filtered Cu Kα radiation operating at 30 mA and 40 kV. Data were recorded in the 5–60° 2θ range (step size 0.019732° and 0.5 s counting time for each step). The relative crystallinity of the samples was determined by the DIFFRAC EVA v4.2 program.

The thermal stability of glasses was analyzed by differential thermal analysis (DTA) up to 1400 °C at a heating rate of 50 °C min^{-1} under flowing air in a Setaram Labsys Thermal Analyzer. Samples of 40 mg were placed in platinum crucibles, and calcined Al_2O_3 was used as the reference material. The DTA curves were normalized with respect to the sample weight.

The microstructure and occurrence of phase separation in the glasses were studied by field emission scanning electron microscopy (FESEM) with a HITACHI S-4800P microscope using an acceleration voltage of 20 kV. Fresh fracture surfaces were etched for 10 s in a solution of 5% HF, ultrasonically washed with distilled water and ethylic alcohol, dried, and coated with Au-Pd in a Balzers SCD 050 sputter.

Finally, the characterization of samples was completed by Fourier transform infrared (FTIR) spectroscopy in Nicolet Nexus 670-870 equipment. FTIR spectra were recorded in the range of 400–4000 cm^{-1} by means of transmission measurements from samples diluted in KBr.

Results and discussion

The macroscopic appearance of all materials obtained by CSP was similar to those obtained by the traditional furnace. In Fig. 2, the glassy aspect of one of the FGs obtained is depicted.

Chemical composition

The chemical composition of the materials determined by XRF is shown in Table 3 (major) and Table 4 (minor components). With respect to the theoretical composition (Table 1), the FG_T glass, prepared in an electric furnace, shows the characteristic variation observed when batches of raw materials are melted in silicon-aluminous crucibles, namely, a considerable increase in the alumina content due to corrosion of the crucible walls by the molten glass. The chemical composition of FG_{15} glass prepared with CSP and with the shortest process time (15 min) is similar to that of the FG_T glass except for the lower alumina content, which indicates lighter corrosion of the crucible. This result is in agreement with that reported by Romero et al. in a study on the melting of ceramic frits with different compositions using CSP [22]. By increasing the CSP processing time from 15 to 35 min, the composition of the obtained glass undergoes important modifications, the most important being the decrease in P_2O_5 and K_2O due to their volatilization during melting. Bourgel et al. [27] studied the gasification of sewage sludge containing 21 wt.% P_2O_5 and highlighted the volatilization of phosphorus in the form of PO and PO_2 (above 1300 °C) and P_2O_5 (above 1400 °C). Moreover, according to Beerkens [28], the kinetics of volatilization of phosphorus from glass melts increase considerably with temperature, so that at 1500 °C, the reaction kinetics are at least two orders of magnitude higher than those at 1000 °C. This behavior has also been observed in the chemical composition of the glass obtained by conventional procedures; in fact, the percentage of phosphorus oxide drops from 17.47 wt.% (theoretical value) to 14.03 wt.% (experimental value). During the melting of the FG_{15} and FG_{35} glasses, 25 wt.% and approximately 60 wt.% of the initial phosphorus is released, respectively. This result indicates that a longer processing time could lead to a higher melting temperature and that the core of the melt probably reached a temperature of over 1500 °C. This finding would also explain the decrease in potassium content as the process time increases, releasing on average almost 50% of the initial potassium content in the glass composition. According to Bourgel et al. [27], the volatilization of potassium as KOH starts in the 1000–1100 °C interval and increases considerably with temperature. KOH evaporation is consequence of the reaction of potassium oxide contained in the glass melt with water vapor at the surface of the melt. The evaporation rate is highly dependent on the composition of the gas atmosphere above the melt [28].

Table 3 – Chemical composition (expressed as oxide wt.%) of glasses obtained by XRF (major components).

Sample	FG_T	FG_{15}	FG_{20}	FG_{30}	FG_{35}
SiO_2	31.60	36.34	42.15	52.43	51.37
P_2O_5	14.03	13.10	10.90	7.15	7.20
CaO	26.53	28.70	27.78	24.14	22.13
K_2O	11.52	12.08	8.59	4.02	6.88
Al_2O_3	8.99	1.91	2.70	4.69	5.21
Na_2O	5.40	5.78	5.84	5.54	5.33
MgO	1.20	1.25	1.26	1.26	1.16

Table 4 – Chemical composition (expressed as oxide wt.%) of glasses obtained by XRF (minor components).

Sample	FG_T	FG_{15}	FG_{20}	FG_{30}	FG_{35}
Fe_2O_3	0.34	0.44	0.47	0.42	0.40
TiO_2	0.08	0.05	0.06	0.07	0.08
SO_3	0.08	0.04	n.d.	n.d.	n.d.
BaO	0.05	0.05	0.05	0.05	0.04
ZnO	0.05	0.03	0.02	0.03	0.02
Cr_2O_3	0.04	0.11	0.12	0.10	0.08
Cl	0.02	0.02	n.d.	n.d.	n.d.
SrO	0.02	0.03	0.03	0.02	0.02
PbO	0.02	0.02	0.01	n.d.	n.d.
MnO	0.01	0.02	0.02	0.02	0.02
CuO	0.01	0.005	n.d.	0.004	n.d.
ZrO_2	0.009	0.05	0.01	0.01	0.01
NiO	0.004	0.006	0.006	n.d.	0.007
Rb_2O	0.004	0.002	n.d.	n.d.	n.d.
MoO_3	0.004	0.003	n.d.	n.d.	n.d.
WO_3	n.d.	0.02	0.02	0.03	0.02

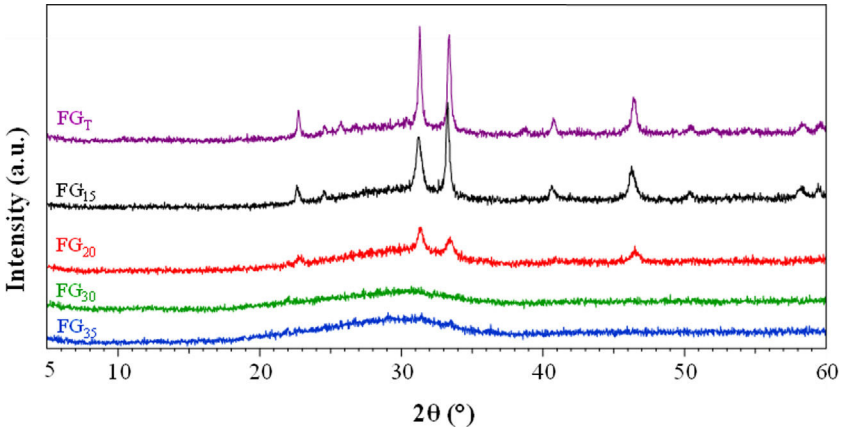

Fig. 3 – XRD patterns of the glasses obtained by CSP (FG_{15}, FG_{20}, FG_{30}, and FG_{35}) and electric furnace (FG_T). The diffraction peaks correspond to $Na_3Ca_6(PO_4)_5$ phase.

Powder X-ray diffraction analysis

The X-ray patterns of the glasses prepared by both CSP and conventional melting are shown in Fig. 3. Concerning the samples melted by CSP, it can be observed that the glassy nature increases as the solar radiation exposure time increases. Thus, for shorter exposure times (15 and 20 min), the materials have a partially glassy nature because a crystalline phase is developed. This phase was identified as sodium and calcium phosphate, $Na_3Ca_6(PO_4)_5$, according to the reference file (ICFF PDF 00-011-0236). The XRD pattern of FG_T exhibits the same XRD profile as that of FG_{15}. This result agrees with the XRF analysis: the glass sample obtained in the electric furnace is similar to that prepared by CSP, although in this case, the reaction time is 90% shorter than the time used in the electric furnace. The decrease in the crystalline nature of the samples as CSP processing time increases is likely related to the reduced availability of groups $(PO_4)^{3-}$ required to develop the crystalline phase during melt cooling since, as mentioned above, an increase in processing time leads to higher volatilization of phosphorus. In fact, Fig. 4 depicts the percentage of $Na_3Ca_6(PO_4)_5$ that could be formed in each sample, considering that all the phosphorus in the glass composition is forming the crystalline

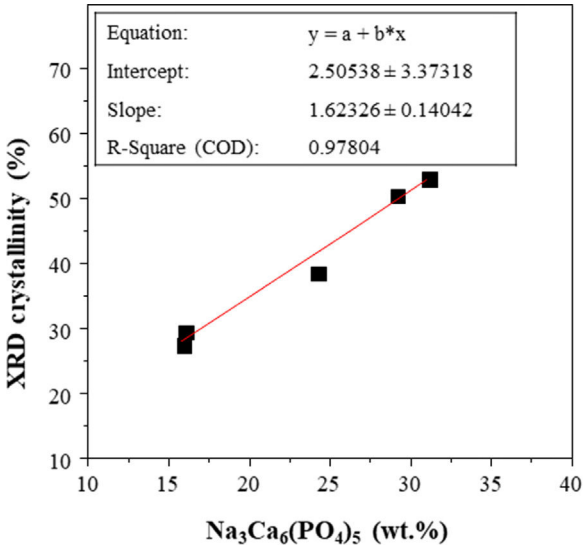

Fig. 4 – Correlation between the percentage of $Na_3Ca_6(PO_4)_5$ possible from the phosphorus content in samples and the percentage of crystallinity.

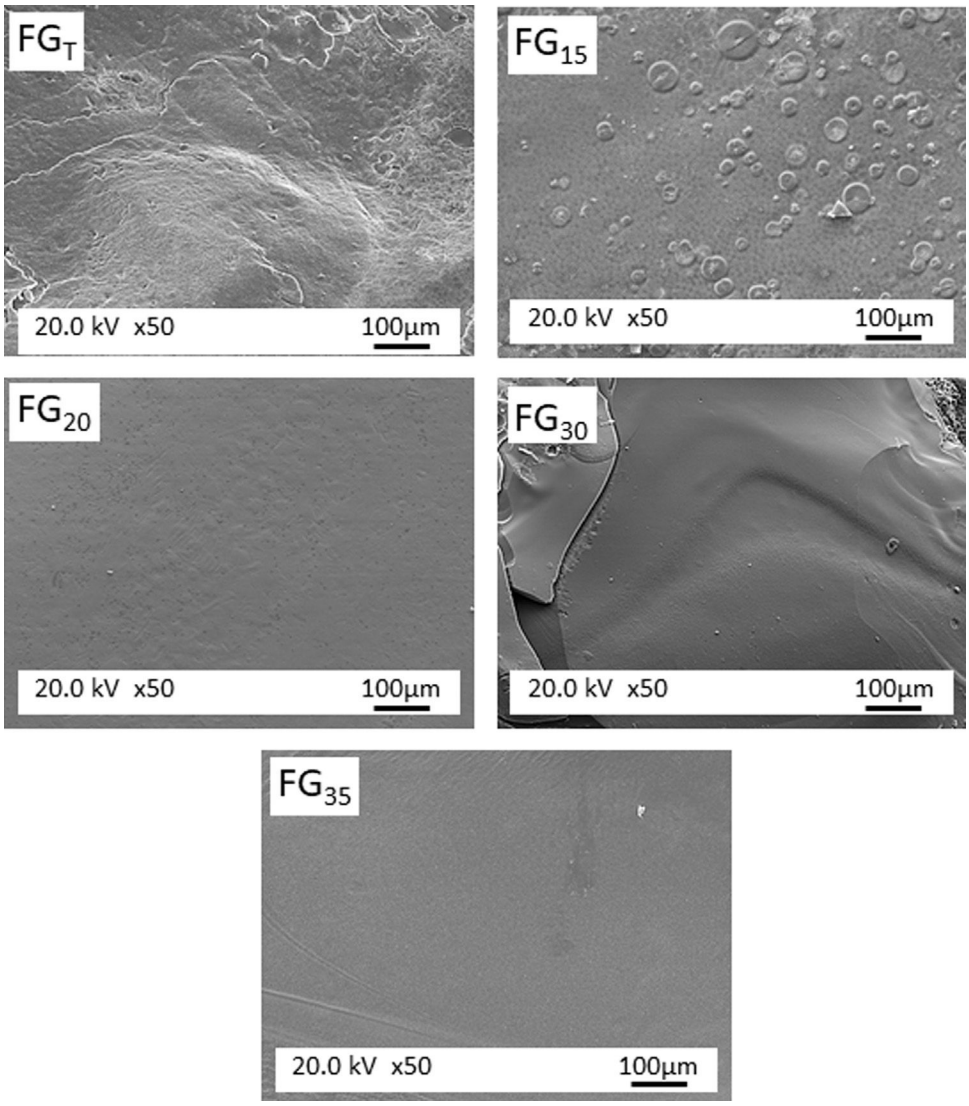

Fig. 5 – Microstructure observed by FESEM on the fresh fracture surface of glasses.

phase, versus the relative crystallinity determined from the X-ray diffractograms. A good correlation between both parameters is obtained. Therefore, the results indicate that in the melting tests carried out with CSP, the increase in the amorphous nature of the samples is due to a decrease in the P_2O_5/CaO and P_2O_5/Na_2O ratios with respect to the stoichiometric ratios necessary for the formation of the $Na_3Ca_6(PO_4)_5$ phase.

Scanning electronic microscopy

Fig. 5 shows the microstructure observed by FESEM on the fresh fracture surface of glasses. The FG_T and FG_{15} glasses show a rough surface due to the precipitation of some $Na_3Ca_6(PO_4)$ crystals, as detected in the XRD spectra (Fig. 3). These crystallizations are visible in glass FG_{15} in the form of spherulites of variable size in the 10–60 µm range. The FG_{20}, FG_{30}, and FG_{35} glasses appear smoother due to the lower content or even lack of crystalline phases and their higher amorphous character (Fig. 3).

Fig. 6 presents FESEM observations of FG_{15} glass at high magnifications. It can be observed that the sample shows a high degree of devitrification and that crystals with a fibroradiated habit have developed during the cooling process. In addition, the intercrystalline matrix shows a high degree of porosity, possibly because of its solubilization during the etching stage preceding FESEM observation. This porous microstructure could also be due to the existence of a residual glass due to a phase separation, caused by a spinodal decomposition mechanism [29], which results in strongly interconnected phases separated by diffuse interfaces. Fig. 7 shows FESEM observations of the FG_{20}, FG_{30}, and FG_{35} glasses, where the absence of crystallization regions allows for better visualization of the microstructure of the glassy phase and the morphology of the spinodal decomposition, which is composed of small globules with sizes smaller than 0.5 µm.

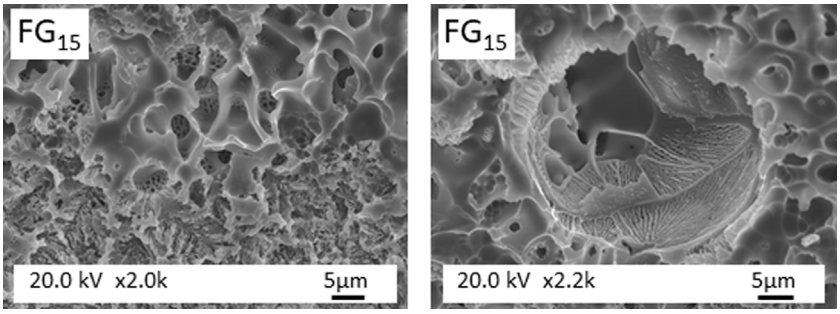

Fig. 6 – High magnification FESEM observations of the fracture surface of FG_{15} glass.

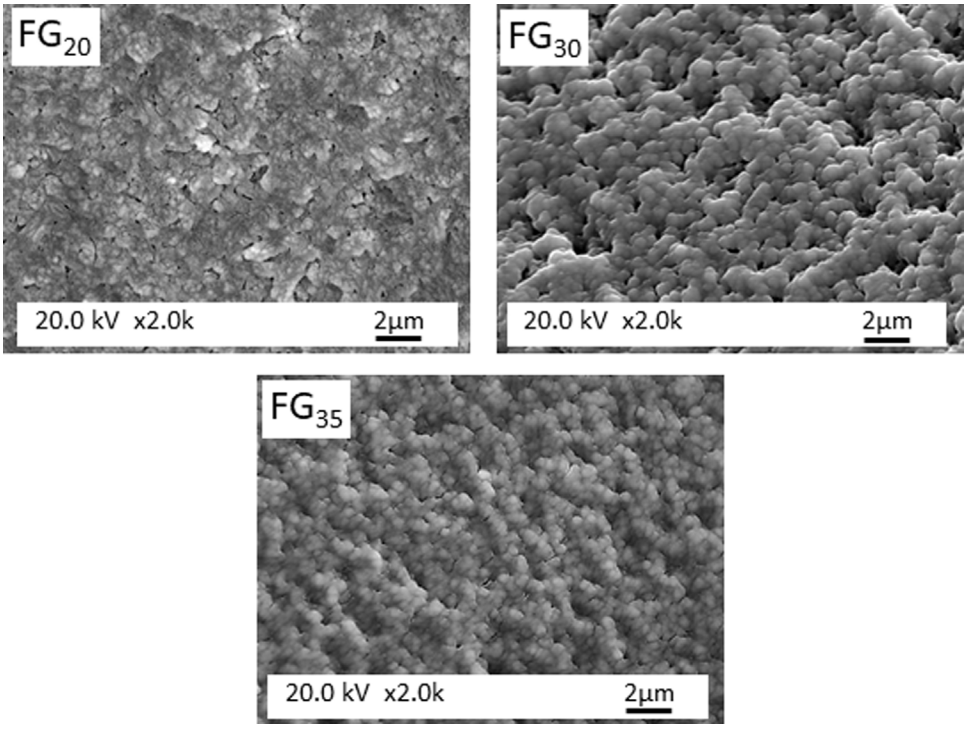

Fig. 7 – High magnification FESEM observations of the fracture surface of FG_{20}, FG_{30}, and FG_{35} glasses.

Thermal analysis

Fig. 8 depicts the DTA curves of the investigated glasses. Some differences in their profiles can be observed, mainly related to the different amorphous/crystalline characters, as shown in Fig. 3. Thus, samples FG_T and FG_{15} are thermally stable, and their DTA curves only show endothermic events corresponding to glass transition temperatures (T_g) of approximately 670 and 630 °C and liquid phase formation with melting temperatures (T_m) of 1155 and 1165 °C, respectively. For the rest of the samples, their DTA curves show an exothermic effect, indicating that the glasses are unstable and that subsequent heat treatments result in a devitrification process and the consequent development of crystalline phases. This result is consistent with the increased amorphous nature of these samples, as shown in Fig. 3. The FG_{35} glass shows the most intense crystallization peak, possibly because crystal development could be favored by the finer morphology of the phase separation.

Table 5 lists the characteristic temperatures for the FG_{20}, FG_{30}, and FG_{35} glasses, namely, T_g, the onset of crystallization temperature (T_x), the temperature of the crystallization peak (T_p), and T_m. For better appreciation, these temperatures were indicated on the DTA curve of the FG_{35} glass (Fig. 8). From these temperatures, different parameters indicative of the stability of the glasses can be determined. Thus, the working range of the glass is an indicator of its thermal stability and is determined by $\Delta T_{TS} = T_x - T_g$ [30]. The narrower this temperature range is, the more complex it is to prevent the occurrence of partial crystallization during the working steps. The thermal stability of FG_{20} glass is very low, probably because this material is not completely amorphous (Fig. 3) and presents a specific structural order that favors the beginning of the development of crystalline phases. On the other hand, longer

Table 5 – Characteristic temperatures (T_g, T_x, T_p, and T_m) and derived parameters for the T_{20}, T_{30}, and T_{35} glasses.

Glass	T_g (°C)	T_x (°C)	T_p (°C)	T_m (°C)	ΔT_{TS} (°C)	T_{gr}	R_c (°C min^{-1})
FG_{20}	643	690	725	1176	47	0.55	38×10^3
FG_{30}	661	810	873	1161	149	0.57	208
FG_{35}	680	841	900	1160	161	0.59	77

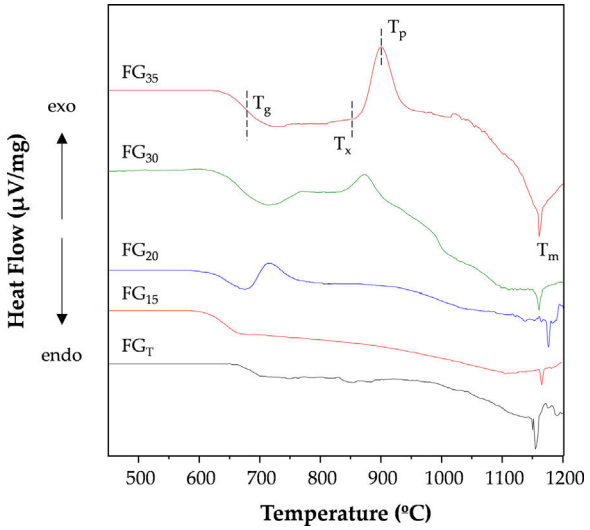

Fig. 8 – DTA curves of the ecofriendly glasses produced by CSP (FG_{15}, FG_{20}, FG_{30}, and FG_{35}) and electric furnace (FG_T).

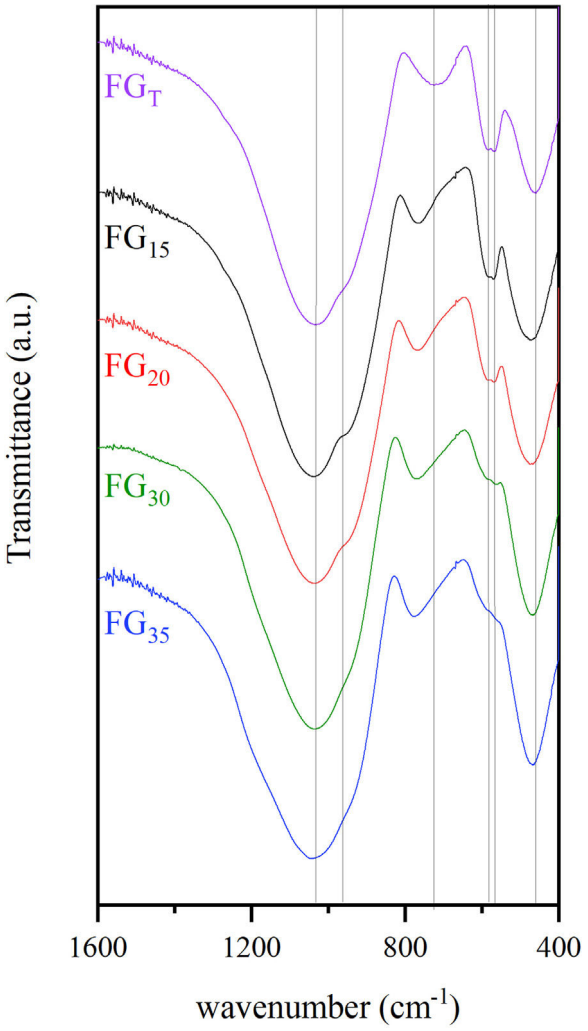

Fig. 9 – FTIR spectra of glasses prepared with concentrated solar radiation (FG_x)) and in an electric furnace (FG_T).

exposure times to concentrated solar radiation lead to glasses with a working range close to or above 150 °C; therefore, it is easy to avoid devitrification during thermal manipulation, e.g., sintering. Another useful parameter is the reduced glass transition temperature, $T_{gr} = T_g/T_m$, which is an indicator of the prevailing crystallization mechanism in the devitrification process. Thus, a T_{gr} value below 0.58 implies the predominance of bulk crystallization, whereas if T_{gr} is above 0.60, crystals develop mainly on the surface of the glass particles. A T_{gr} value in the range 0.58–0.60 denotes no distinctly predominant mechanism. In the FG_{20}, FG_{30}, and FG_{35} glasses, the crystallization mechanism in volume plays a predominant role, but surface crystallization also becomes important in the glasses manufactured with the highest exposure times to concentrated solar energy.

On the other hand, the glass-forming ability (GFA) is the capability of a melt to become glass during cooling, and it can be assessed by the critical cooling rate, R_c, which is the slowest rate from melting to T_g, to avoid crystallization. R_c can be determined as $\log_{10} R_c = 17.7 - 34.6\,K_{LL}$, where K_{LL} is the Lu-Liu parameter and $K_{LL} = T_x/(T_g + T_m)$ [31,32]. The R_c values in Table 5 indicate that FG_{20} presents a high tendency to crystallize during cooling, and therefore, a very fast cooling rate would be necessary to achieve a completely amorphous material. This result is in agreement with the mineralogical study (Fig. 3), which revealed the semi crystalline character of this glass, even though the melt was quenched by pouring in cold water. As the exposure time to concentrated solar power increases, the melts become more stable, and the critical cooling rate decreases considerably so that glasses obtained with 35 min of exposure can be cooled to a rate lower than 100 °C min^{-1} without causing the atomic rearrangement necessary for the development of a crystalline phase.

FTIR spectroscopy

Fig. 9 shows FTIR transmission spectra of glass samples produced by CSP (FG_{15}, FG_{20}, FG_{30}, and FG_{35}) and by an electric furnace (FG_T). In general, the spectra of the different samples are quite similar, and they show some specific bands within the range 400–1600 cm^{-1} characteristic of phosphate-silicate glasses. The most intense band appears at 1035 cm^{-1},

Table 6 – FTIR bands assignment.

FG_T	FG_{15}	FG_{20}	FG_{30}	FG_{35}	Assignment
					ν_{as}
1031 vs b	1035 vs b	1035 vs b	1043 vs b	1035 vs b	Si-O-Si
960 sh	969 sh	956 sh	955 sh	954 sh	P-O-Si
					P-O-P
					ν_s
					Si-O-Si
724 w	765 w	768 w	777 w	769 w	P-O-Si
					P-O-P
					δ
584 m	581 m	583 m	585 w	584 w	P-O
568 m	569 m	573 m	559 w	564 w	(PO_{43}-)
					δ
460 s	472 s	475 s	468 s	468 s	Si-O/P-O

which is very broad because of the superposition of several bands situated close to each other [33–35]. These bands are attributed to the asymmetric stretching vibrations of bridging oxygen atoms in Si—O—Si, Si—O—P, and P—O—P bonds. A shoulder at approximately 960 cm^{-1} can also be detected in all glasses. Bands at approximately 724–777 cm^{-1} can be attributed to symmetric stretching vibrations of the Si—O—Si, Si—O—P, and P—O—P bonds. Several differences are observed in the position of these bands according to the use of solar or conventional processes for the melting of glasses. Thus, the band at 724 cm^{-1} in sample FG_T is shifted toward higher wavenumbers for samples obtained by CSP. This can be attributed to the higher content of glass framework former, i.e., SiO_2 and P_2O_5, especially SiO_2, which is higher in glasses obtained by CSP than in samples obtained by electric furnace (Table 3). The FTIR spectrum of sample FG_T shows a set of double bands at 584 and 568 cm^{-1}, which are related to the deformation vibrational mode of the tetrahedral phosphate group [35,36]. The higher P_2O_5 content, the more intensity of this band. Thus, the intensity of this band is higher for samples in which $Na_3Ca_6(PO_4)$ was observed as a crystalline phase (FG_T, FG_{15}, and FG_{20}) than in samples FG_{30} and FG_{35} with an XRD profile without any crystalline phase. Finally, the bands observed at approximately 460–475 cm^{-1} are assigned to combinations of bending modes of O—Si—O and O—P—O bonds. These bands are shifted to higher wavenumbers for samples obtained by CSP, especially for glass with a higher content of glass structure modifiers such as CaO (FG_{15} and FG_{20}).

Table 6 collects the tentative assignment of the different FTIR bands for all samples according to the literature.

Conclusions

A mixture of animal bone flour ash (40 wt.%), glassy sand (42 wt.%) and K_2CO_3 (18 wt.%) was melted by both a conventional process in an electric furnace and a process involving concentrated solar energy. Based on the results of the characterization tests performed on the materials resulting from melting, the following conclusions can be drawn:

- The use of CSP reduces the processing time considerably since the material prepared with a processing time of 15 min has a chemical composition and mineralogy similar to that prepared by a conventional process (almost 5 h).
- An increased CSP processing time leads to increased volatilization of phosphorus and potassium, likely due to reaching working temperatures above 1500 °C.
- The glass melted in a conventional furnace (FG_T), and the FG_{15} glass prepared by CSP with 15 min exposure show a glass-ceramic nature due to the development of $Na_3Ca_6(PO_4)_5$ during the cooling of the melt.
- The increased CSP processing time results in a more amorphous nature of the final materials because of the reduced availability of $(PO_4)^{3-}$ units for crystal phase formation.
- $Na_3Ca_6(PO_4)_5$ develops in the form of spherulites with fibro-radiated habits, and the glassy phase presents a phase in phase spinodal decomposition.
- The increased CSP processing time also leads to more thermally stable melts and glasses.

In brief, the results of this study highlight the viability of producing ecofriendly glasses in the SiO_2–P_2O_5–CaO–K_2O system by using different wastes (viz. animal bone flour ash as the CaO and P_2O_5 source and glassy sand as the SiO_2 source) and concentrated solar energy as the renewable energy source. According to their chemical composition and characteristics, these glasses could be used as matrix-based fertilizers.

Acknowledgments

The authors thank The European Solar Research Infrastructure for Concentrated Solar Power SFERA-III program (EU. DG RTDs) for providing the infrastructure used to develop project FIGARO-SURPF1904010021. The authors would like to acknowledge Dr. J.I. Robla for his highly valuable and significant assistance in the melting of glasses by concentrated solar power. The collaboration of Ms. P. Díaz and Ms. E. Martín in the preparation of the samples for characterization is also appreciated.

REFERENCES

[1] F. Andreola, A. Borghi, S. Pedrazzi, G. Allesina, P. Tartarini, I. Lancellotti, L. Barbieri, spent coffee grounds in the production of lightweight clay ceramic aggregates in view of

urban and agricultural sustainable development, Materials 12 (21) (2019) 3581.
[2] M.K. Enriquez, J.I. Tobon, J.H. Ramirez, Use of industrial wastes for the synthesis of belite clinker, Mater. Constr. 70 (339) (2020) e226.
[3] R.D. Farias, C.M. Garcia, T.C. Palomino, F. Andreola, I. Lancellotti, L. Barbieri, Valorization of agro-industrial wastes in lightweight aggregates for agronomic use: preliminary study, Environ. Eng. Manag. J. 16 (8) (2017) 1691–1699.
[4] F. Andreola, I. Lancellotti, T. Manfredini, L. Barbieri, The circular economy of agro and post-consumer residues as raw materials for sustainable ceramics, Int. J. Appl. Ceram. Technol. 17 (1) (2020) 22–31.
[5] G. Thalmaier, N. Cobirzan, A.A. Balog, H. Constantinescu, M. Streza, M. Nasui, B.V. Neamtu, Influence of sawdust particle size on fired clay brick properties, Mater. Constr. 70 (338) (2020) e215.
[6] K. Belhouchet, A. Bayadi, H. Belhouchet, M. Romero, Improvement of mechanical and dielectric properties of porcelain insulators using economic raw materials, Bol. Soc. Esp. Ceram. Vidr. 58 (1) (2019) 28–37.
[7] S.S. Owoeye, T.S. Toludare, O.E. Isinkaye, U. Kingsley, Influence of waste glasses on the physico-mechanical behavior of porcelain ceramics, Bol. Soc. Esp. Ceram. Vidr. 58 (2) (2019) 77–84.
[8] L. Koroglu, C. Peksen, The effect of particle size and phosphorous content in biomineralization media on in vitro bioactivity of monticellite based ceramic powders obtained from boron derivative waste, Bol. Soc. Esp. Ceram. Vidr. 60 (2) (2021) 93–108.
[9] A. Manni, A. El Haddar, I.E.E. El Hassani, A. El Bouari, C. Sadik, Valorization of coffee waste with Moroccan clay to produce a porous red ceramics (class BIII), Bol. Soc. Esp. Ceram. Vidr. 58 (5) (2019) 211–220.
[10] D. Suarez-Riera, A. Merlo, L. Lavagna, R. Nistico, M. Pavese, Mechanical properties of mortar containing recycled *Acanthocardia tuberculata* seashells as aggregate partial replacement, Bol. Soc. Esp. Ceram. Vidr. 60 (4) (2021) 206–210.
[11] V. Flores-Ales, M. Rodriguez-Romero, I. Romero-Hermida, L. Esquivias, Characterization of mixed mortars with lime obtained from recycled phosphogypsum, Bol. Soc. Esp. Ceram. Vidr. 59 (3) (2020) 129–136.
[12] A. Mourak, M. Hajjaji, A. Alagui, Cured alkali-activated heated clay-cellulose composites: microstructure, effect of glass addition and performances, Bol. Soc. Esp. Ceram. Vidr. 60 (1) (2021) 62–72.
[13] K.A. de Oliveira, C.A.B. Oliveira, J.C. Molina, Lightweight recycled gypsum with residues of expanded polystyrene and cellulose fiber to improve thermal properties of gypsum, Mater. Constr. 71 (341) (2021) e242.
[14] E. Ferraz, J.A.F. Gamelas, J. Coroado, C. Monteiro, F. Rocha, Exploring the potential of cuttlebone waste to produce building lime, Mater. Constr. 70 (339) (2020) e225.
[15] American National Oceanic and Atmospheric Administration. https://www.esrl.noaa.gov/gmd/ccgg/trends/global.html (accessed October 2021).
[16] SDGs, Sustainable Development Goals, 2021. https://www.un.org/sustainabledevelopment/ (accessed October 2021).
[17] M.F. Barba, P. Callejas, J.O. Arzabe, D. Ajo, Characterization of two frit ceramic materials as low cost fertilizers, J. Eur. Ceram. Soc. 18 (9) (1998) 1313–1317.
[18] I. Waclawska, A. Szumera, Reactivity of silicate-phosphate glasses in soil environment, J. Alloys Compd. 468 (1–2) (2009) 246–253.
[19] C.F. Drake, Water soluble glass and its use in controlled release of chemical species, E.P. Office (1980).
[20] B.A. Sava, L. Boroica, M. Sava, M. Elisa, C.I. Vasiliu, F. Nastase, C. Nastase, R. Medianu, Potassium phosphate glasses used as agro-fertilizers with controlled solubility, J. Optoelectron. Adv. Mater. 13 (11–12) (2011) 1534–1541.
[21] I. Padilla, M. Romero, J.I. Robla, A. López-Delgado, Waste and solar energy: an eco-friendly way for glass melting, ChemEngineering 5 (2) (2021) 16.
[22] M. Romero, J. Robla, I. Padilla, J. Garcia-Hierro, A. Lopez-Delgado, Eco-efficient melting of glass frits by concentrated solar energy, Sol. Energy 174 (2018) 321–327.
[23] L. Barbieri, F. Andreola, D. Bellucci, V. Cannillo, I. Lancellotti, A. Lugari, J.M. Rincon, M. Romero, A. Sola, Preliminary studies on the valorization of animal flour ash for the obtainment of active glasses, Ceram. Int. 40 (4) (2014) 5619–5628.
[24] D. Ronga, M. Parisi, L. Barbieri, I. Lancellotti, F. Andreola, C. Bignami, Valorization of spent coffee grounds, biochar and other residues to produce lightweight clay ceramic aggregates suitable for nursery grapevine production, Horticulturae 6 (4) (2020) 58.
[25] S. Barbi, F. Barbieri, F. Andreola, I. Lancellotti, L. Barbieri, M. Montorsi, Preliminary study on sustainable NPK slow-release fertilizers based on byproducts and leftovers: a design-of-experiment approach, ACS Omega 5 (42) (2020) 27154–27163.
[26] B.M. Scalet, M. García Muñoz, A. Sissa, S. Roudier, L. Delgado Sancho, Best available techniques for the manufacture of glass, Publications Office of the European Union (2012).
[27] C. Bourgel, E. Veron, J. Poirier, F. Defoort, J.M. Seiler, C. Peregrina, Behavior of phosphorus and other inorganics during the gasification of sewage sludge, Energy Fuels 25 (12) (2011) 5707–5717.
[28] R.G.C. Beerkens, Modeling the kinetics of volatilization from glass melts, J. Am. Ceram. Soc. 84 (9) (2001) 1952–1960.
[29] O.V. Mazurin, E.A. Porai-Koshits, Phase Separation in Glass, North-Holland, Amsterdam, Oxford, New York, Tokyo, 1984.
[30] I.W. Donald, B.L. Metcalfe, L.A. Gerrard, S.K. Fong, The influence of Ta_2O_5 additions on the thermal properties and crystallization kinetics of a lithium zinc silicate glass, J. Non-Cryst. Solids 354 (2–9) (2008) 301–310.
[31] Z.P. Lu, C.T. Liu, A new glass-forming ability criterion for bulk metallic glasses, Acta Mater. 50 (13) (2002) 3501–3512.
[32] Z.P. Lu, C.T. Liu, Glass formation criterion for various glass-forming systems, Phys. Rev. Lett. 91 (11) (2003) 115505.
[33] B. Lagowska, I. Waclawska, M. Sitarz, M. Szumera, Spectroscopic studies of structural interactions in silicate-borate phosphate glass, J. Mol. Struct. 1171 (2018) 110–116.
[34] N. Saloumi, M. El Bouchti, Y. Tamraoui, B. Manoun, L.H. Hannache, O. Cherkaoui, Structural, chemical and mechanical properties of phosphate glass fibers, J. Non-Cryst. Solids 522 (2019) 119587.
[35] M. Szumera, I. Waclawska, W. Mozgawa, M. Sitarz, Spectroscopic study of biologically active glasses, J. Mol. Struct. 744 (2005) 609–614.
[36] O.J. Eddine, H. Wakrim, M. El Bouchti, A. Boukhriss, O. Cherkaoui, H. Hannache, S. Gmouh, Effect of the chemical composition on the structural and mechanical properties of phosphate glass fibers based on natural phosphate, J. Alloys Compd. 817 (2020) 152808.